Electronic Supplementary Material (ESI) for Environmental Science: Nano.
This journal is © The Royal Society of Chemistry 2024

Ultrathin Defective Heterojunction for Visible Light NO Removal: Correlation between Microstructure and Reaction Mechanisms

Reshalaiti Hailili,[a,b,c*] Zelong Li,[a] Xu Lu,[a] Hua Sheng,[b*] Detlef W. Bahnemann,[c] Jincai Zhao[b]

[a]*MOE Key Laboratory of Enhanced Heat Transfer and Energy Conservation, Beijing Key Laboratory of Heat Transfer and Energy Conversion, Beijing University of Technology, Beijing 100124, P. R. China.*

[b]*Key Laboratory of Photochemistry, Institute of Chemistry, Chinese Academy of Sciences, Beijing 100190, P. R. China.*

[c]*Institut für Technische Chemie, Gottfried Wilhelm Leibniz Universität Hannover, Callinstr. 3, 30167 Hannover, Germany.*

[*]Corresponding authors:

Reshalaiti100@163.com (R. Hailili); hsheng@iccas.ac.cn (H. Sheng)

Table S1. Magnitude Debye of polyhedra in the minimum asymmetric unit of $BiVO_4$.

	$BiVO_4$ (Dipole moment)			
symmetric	x	y	z	Magnitude (D)
BiO_6 (x, y, z)	0.095	0.052	12.77	12.77

2. Experimental Section

Synthesis of $BiVO_4$ monomers: 10.0 mL glyoxal/water was subsequently added into the above solution and underwent further stirring for 20 min to obtain a uniform solution. Upon vigorous stirring, pre-dissolved NH_4VO_3 was added to the above solution dropwise and kept magnetic stirring for another 30 min. Following this step, 10 mL of 1.0 M NaOH aqueous solution was added to the above solution to adjust the pH of the solution to 7.0 upon stirring. After that, the suspension was carefully transferred into a Teflon-lined stainless-steel autoclave, heated at 150 ^{o}C with an increase of 2 ^{o}C/min and kept for 12 h at autogenous pressure.

Synthesis of BiOCl monomers: For the synthesis of BiOCl monomer, 1.0 mmol $Bi_2(NO_3)_3{\cdot}6H_2O$ and 0.5 g PVP were dissolved in 10.0 mL glyoxal/water and underwent vigorous stirring for about 40 min. Upon continuous stirring, 4.5 mL saturated NaCl solution was carefully dropped into the solution as a Cl^- source and stirred for another 40 min. Then, a white precipitate was obtained and further washed with deionized water until the pH reached neutral. After that, the as-obtained mixture was transferred into the Teflon-lined stainless-steel autoclave, and further treated at 150 ^{o}C for 4 h.

Synthesis of defect-free $BiVO_4$/BiOCl photocatalysts: The synthesis of defect-free $BiVO_4$/BiOCl heterojunction is the same as defective heterojunction except for the absence of reducing agent glyoxal/water.

Characterizations. The crystal structure of as-studied photocatalysts was analyzed by X-ray Powder Diffraction (XRD) measurements, which were carried out on a Bruker D8 ADVANCE X-ray diffractometer in the angular range of 2θ = 5° ~ 80° with a scan step width of 0.02° and a fixed counting time of 1 s/step using Cu Kα radiation (λ = 1.5418 Å). The light absorption was analyzed by using a Shimadzu Solidspec-3700 DUV Uv−vis spectrophotometer. The accurate amounted catalysts (45.0 mg) were further diluted by reference $BaSO_4$ and analyzed within the wavelength range of 200 nm−800 nm. A reference $BaSO_4$ was used for a baseline correction before the measurements. The structure and morphology analyses were performed by a scanning electron microscope (SEM) observation on a Hitachi S-3500N SEM. Further microstructure characters were investigated by transmission electron microscopy (TEM) and high-resolution TEM (HRTEM, JEOL-JEM 2100). Atomic force microscopy (AFM) measurements were performed to measure the thickness by using Bruker Dimention edge AFM (GER). The stabilities of the defects on the surfaces of as-investigated samples were analyzed by electron paramagnetic resonance (EPR) and XRD

measurements after long-term visible light NO conversion tests of samples.

Photocatalytic NO removal. In a typical procedure, the same amount of precisely measured photocatalyst (65.0 mg) was pretreated at 100 ^{o}C for 2 h to remove surface adsorbed species, then was uniformly dispersed in the distilled water to obtain a suspension. As dispersed slurry photocatalysts were further deposited in a specially designed glass dish, underwent ultrasonication for 12.0 min, and further dried at 60 ^{o}C. Then this was positioned in a designed reactor and subsequently supported by the sample holder. The vertical distance between the light and the catalyst surface was about 15.0 cm. The NO gas (13.5 ppm, balance with Ar, 99.999%) was obtained from a compressed gas cylinder from the National Institute of Standards and Technology specifications. With a continuous flow rate of 1.0 L·min^{-1} by a mass flow controller, the NO gas was diluted by an air stream supplied by a zero-air generator to obtain the precise concentration of 500 ppb, which was completely premixed by a gas blender, accessed to the chamber and passed over the powder surface through the inlet tube. For all tests, as-obtained catalysts were suspended to the gas stream and stabilized for 30.0 min without light illumination to achieve constant gas concentration and adsorption−desorption balance.

Temperature-programmed desorption (TPD). The TPD of the target NO over 180.0 mg/per sample was measured on a Quantachrome Autosorb-IQ-MP system, which was equipped with a TCD detector. A predesigned temperature program was employed before the measurements to clean and remove the possible adsorbents on samples. In detail, precisely weighted samples were heated from room temperature up to 300 ^{o}C at a heating rate of 10 ^{o}C·min^{-1} and kept at 300 ^{o}C for 60 min, then the samples were subsequently cooled to 50 ^{o}C and kept for 30 min. All this procedure was conducted under the continuous Ar flow (120.0 mL·min^{-1}). After that, the Ar gas flow was switched to NO and kept for 60 min to establish the adsorption equilibrium. Then, the gas flow was changed back to the Ar again to remove the gaseous NO in the system, following measurements of TPD for NO proceeded when the temperature increased from 50 ^{o}C to 800 ^{o}C at a rate of 10 ^{o}C·min^{-1}.

Photo-electrochemical tests. The photocurrents were performed on an electrochemical workstation (CHI 600E) with a standard three-electrode system, in which Pt was used as a counter electrode. As-synthesized catalyst-deposed indium-tin-oxide (ITO) glass substrate was used as working electrodes, and Ag/AgCl electrodes in KCl saturated solution were employed as reference electrodes, respectively. In the typical preparation of working electrodes, identical amounts of precisely

measured catalysts were dispersed in ethanol and water solution with the assistance of Nafion solution (300 μL, 4.0 wt %) to form a homogeneous slurry. Then, the obtained pasty catalysts were deposed on the surface of ITO glass and dried naturally. A 0.20 M Na_2SO_4 solution was used as the electrolyte, and the 300 W Xenon lamp ($\lambda \geq 420$ nm) was used as a light source as was used in the activity assessment test. All the experiments were carried out at room temperature.

***In situ* Diffused Reflectance Infrared Fourier Transform (DRIFTS).** *In situ* DRIFTS measurements were conducted using a TENSOR II FT-IR spectrometer (Bruker) equipped with an *in situ* diffuse-reflectance cell (Harrick). High-purity He, high-purity O_2, and 100 ppm of NO (in He) mixtures were fed into the reaction system, and a three-way ball valve was used to switch between the target gas (NO) and purge gas (He). A Xe lamp (MUA-210, Japan) was used as the light source. Before the measurements, as-synthesized photocatalysts were pretreated 30 min at 300 ^{o}C in the high-temperature reaction chamber. The background spectrum is recorded before injecting reactant gas into the reaction chamber. Once the adsorption equilibrium is achieved, a visible light source is applied to initiate the photocatalytic reaction.

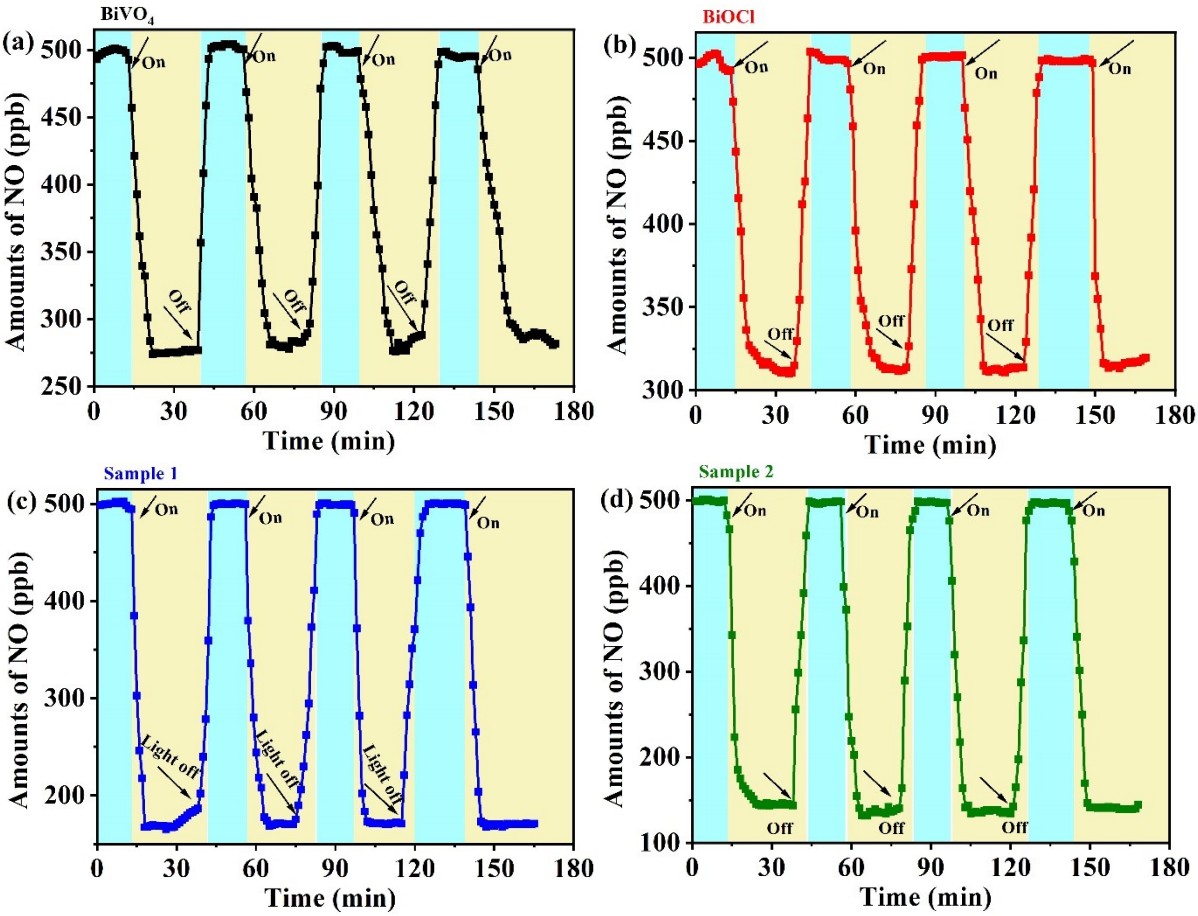

Fig. S1. Long-term photocatalytic NO removal in the presence of as-investigated samples for four cycles.

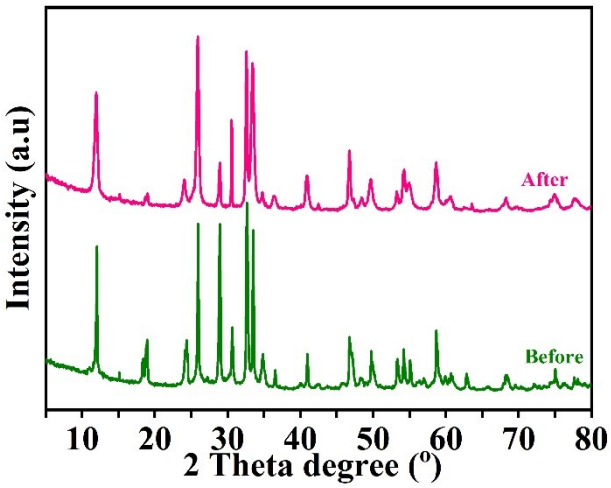

Fig. S2. Comparative XRD patterns of as-constructed defective heterojunction (Sample 2) before and after the Long-term photocatalytic NO removal tests.

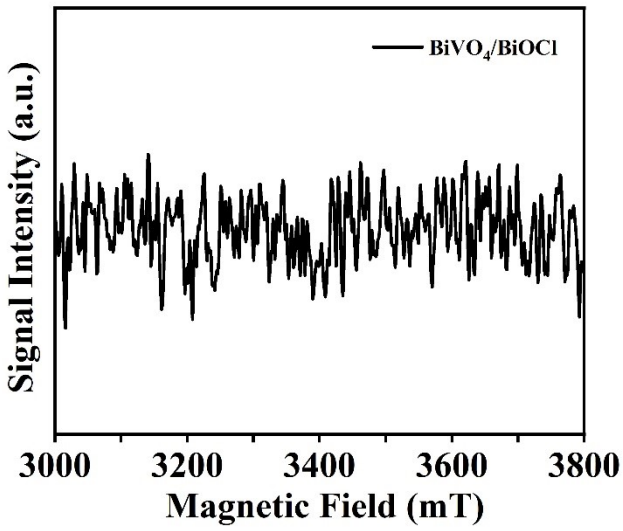

Fig. S3. Room-temperature EPR profiles of as-synthesized defect-free $BiVO_4$/BiOCl.

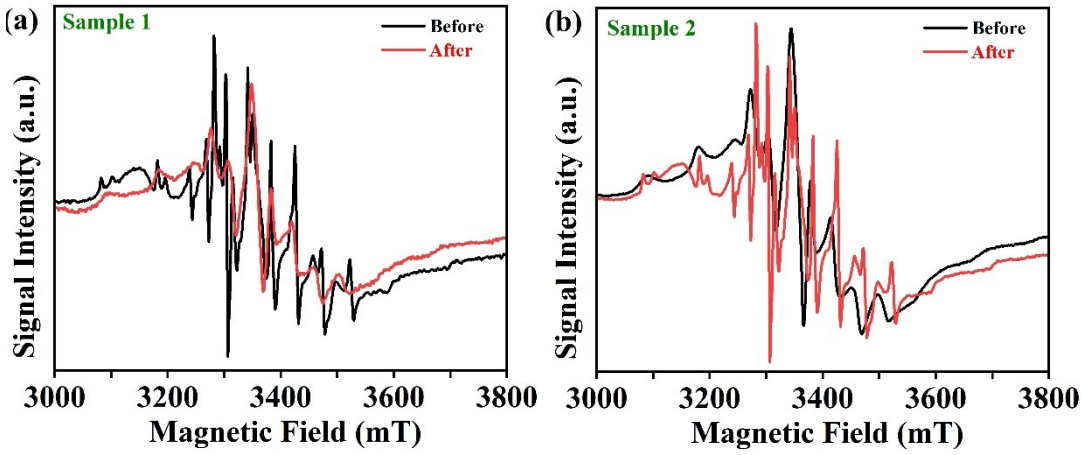

Fig. S4. Comparative results of room-temperature EPR profiles of sample 1 and sample 2 photocatalysts before and after the four-runs of NO removal tests, respectively.

3. "N Balance" Calculations

The concentration of NO_3^- detected by ion chromatography in the washing solution of used BiOCl, $BiVO_4$, $BiVO_4$/BiOCl (sample 1), and $BiVO_4$/BiOCl (sample 2) were 2.9347, 4.129, 1.859, and 2.138 μg/L, respectively.

A. The computational formula of the consumption of NO (C_{NO}) is $C_{NO=} \sum_{t=1}^{t=45} NO$; the results in BiOCl, $BiVO_4$, $BiVO_4$/BiOCl (sample 1), and $BiVO_4$/BiOCl (sample 2) were 15.365, 17.166, 11.835, and 10.6255 ppm, respectively.

The computational formula of concentration of consumed NO (C_{NO}) is $C_{NO} = \frac{30 \times C_{NO}}{22.4}$; the results in BiOCl, $BiVO_4$, $BiVO_4$/BiOCl (sample 1), and $BiVO_4$/BiOCl (sample 2) were 20.57, 22.99, 15.85, and 14.23 μg/L, respectively.

B. The generated NO_2 (C_{NO2}) is: $C_{NO2=} \sum_{t=1}^{t=45} NO_2$; the results in BiOCl, $BiVO_4$, $BiVO_4$/BiOCl (sample 1), and $BiVO_4$/BiOCl (sample 2) were 2.42, 0.39, 3.88, and 1.16 ppm, respectively.

The concentration of NO which converted to NO_2 (CNO/NO_2) is $(C\frac{NO}{NO_2}) = \frac{30 \times C_{NO2}}{22.4}$; the results in BiOCl, $BiVO_4$, $BiVO_4$/BiOCl (sample 1), and $BiVO_4$/BiOCl (sample 2) were 3.25, 0.52, 5.198, and 1.55 μg/L, respectively.

C. The concentration NO which converted to NO_3^- is $(C\frac{NO}{NO_3}) = \frac{NO_3}{62} \times 30$; the results in in BiOCl, $BiVO_4$, $BiVO_4$/BiOCl (sample 1), and $BiVO_4$/BiOCl (sample 2) were 14.12, 19.98, 8.996, and 11.212 μg/L, respectively.

D. The values of $C_{NO/NO3}$ + $C_{NO/NO2}$ in different samples were approximately equal to that of consumption NO (C_{NO}). Therefore, the formed NO_2, and NO_3 can meet with the consumed NO.

Table S2. Assignments of the IR bands observed on samples during the photocatalytic NO removal.

Wavenumbers (cm^{-1})	Assignment	References
908	N_2O_4	S1
991	bi-NO_3^-	S2
1034	bi-NO_3^-/ mo-NO_2^-	S3
1072	bi-NO_3^-/ mo-NO_2^-	S3
1111	bi-NO_2^-	S3-4
1237	bi-NO_3^-	S3-4
1378	free nitrates	S5
1432	bi-NO_3^-	S6
1495	bridging NO_2^-	S3
1635	bridging NO_2^-	S3

Table S3. Summary of synthesis, microstructures, photocatalytic performances and proposed reaction mechanisms of $BiVO_4$/BiOCl heterojunctions.

Photocatalyst	Synthetic method	Microstructures	Light source	Catalyst Dosage	Photo performance	Mechanisms	Reference
BiOCl-$BiVO_4$	Photo-deposited crystal plane selectively induce method	BVO_4 nanosheets and BiOCl nanoparticles on (010) and (110) facet of BVO	500 W xenon lamp (400-800 nm)	50 mg	TC (40 mg/L), 180 min, 90.32% CIP, BHA, phenol, BPA, coumarin (10 mg/L), 180 min: 71.32%,49.36%, 65.69%, 57.20%, 57.52%	S-type and Z-type heterojunction 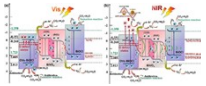	S7
BiOCl-$BiVO_4$:Er^{3+}, Yb^{3+}	electrospinning combined with a solvothermal method	BiOCl nanosheets on $BiVO_4$:Er^{3+}, Yb^{3+} nanobelts	200 W xenon lamp	20 mg, 50 mg	MB (10 mg/L), 120 min, 97.9% TC (10 mg/L), 60 min, 88.8% BPA (10 mg/L), 180 min, 80.8%	S-type heterojunction 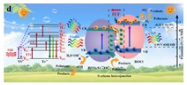	S8
BiOCl-$BiVO_4$	solvothermal method	$BiVO_4$ nanosheets /BiOCl microsphere	500 W halogen bulb (＞420 nm)	5 mg, 25 mg, 50mg	RhB (10 ppm), 105 min, 98.82% TC (20 ppm), 70 min, 73.21% $K_2Cr_2O_7$ (10 ppm), 105 min, 68.53%	Z-type heterojunction 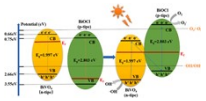	S9
Au-(BiOCl-$BiVO_4$)	coprecipitation method	sphere and elongated-shapes	170 W LED lamp (430-620 nm)	250 mg	MO (10 mg/L), 240 min, 67%	p-n heterojunction 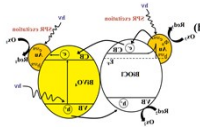	S10
BiOCl-$BiVO_4$	one-pot combustion method	flower-like morphology	300 W xenon lamp (＞450 nm)	100 mg	RhB (20 mg/L), 180 min, 85%	p-n heterojunction 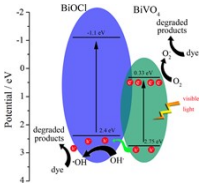	S11
BiOCl-$BiVO_4$	hydrothermal treatment	hierarchical microspheres	Xenon lamp (＞400 nm)	100 mg	RhB (10 mg/L), 4 h, 100%	p-n heterojunction	S12

						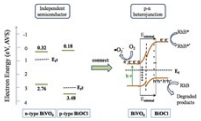	
$BiOCl-BiVO_4$	in situ chemical transformation	BiOCl sheets and $BiVO_4$ nanoparticles	500 W xenon lamp (>420 nm)	100 mg	RhB (20 mg/L), 210 min, 93%	p-n heterojunction 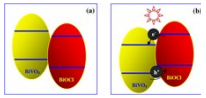	S13
$Bi-BiOCl-BiVO_4$	hydrothermal method	nanosheets	300 W xenon lamp (>420 nm)	200 mg	RhB (8 mg/L), 40 min, 100%	p-n heterojunction 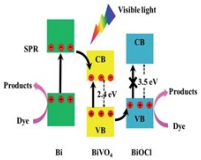	S14
$BiOCl-BiVO_4$	deposition–precipitation method	BiOCl nanoflakes / m-$BiVO_4$	500W xenon lamp (>420 nm)	100 mg	MO (10 mg/L), 6 h, 97.4%	p-n heterojunction 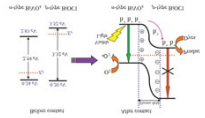	S15
$BiOCl-AgCl-BiVO_4$	one-pot hydrothermal method	square nanoplates	60 W LED lamp (>420 nm)	1 g/L	DCF (5 mg/L), 2.5 h, 72%	p-n heterojunction	S16
BiOCl (110)-NrGO-$BiVO_4$	hydrothermal method	BiOCl nanoplates / leaf $BiVO_4$ on NrGO layers	150 W xenon lamp (<420 nm)	50 mg/L	SMZ (15 mg/L), 60min, 96.9%	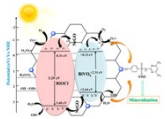	S17
$BiVO_4-BiOCl-Bi_2S_3$	Sonochemical method	irregular shapes	300 W xenon lamp (>420 nm)	100 mg	RhB (10 μM), 20 min, 100%	p-n heterojunction 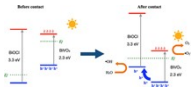	S18
Defective $BiVO_4$-BiOCl	hydrothermal method	BiOCl sheets / $BiVO_4$ nanoparticles	300 W xenon lamp (>420 nm)	65 mg	NO (500 ppb), 45 min, 74.51%	Z-type heterojunction	This work

Note: CIP-Ciprofloxacin; TC-tetracycline; BHA-salicylic acid; BPA-bisphenol a; MB-methylene blue; RhB-Rhodamine b; MO-methyl orange; DCFF-diclofenac; SMZ-sulfamethazine

References

[S1] L. Jaan, J. R. Ohlsen, Characterization of Nitrogen Oxides by Vibrational Spectroscopy, 2007, p 465-513.

[S2] G. Ramis, G. Busca, V. Lorenzelli, P. Forzatti, Fourier Transform Infrared Study of the Adsorption and Coadsorption of Nitric Oxide, Nitrogen Dioxide and Ammonia on TiO_2 Anatase, *Appl. Catal. B*, 1990, **64**, 243-257.

[S3] M. Kantcheva, Identification, Stability, and Reactivity of NO_x Species Adsorbed on Titania-Supported Manganese Catalysts, *J. Catal.*, 2001, **204**, 479-494.

[S4] K. Hadjiivanov, V. Avreyska, D. Klissurski, T. Marinova, Surface Species Formed after NO Adsorption and NO + O_2 Coadsorption on ZrO_2 and Sulfated ZrO_2: An FTIR Spectroscopic Study, *Langmuir*, 2022, **18**, 1619-1625.

[S5] L. Zhong, Y. Yu, W. Cai, X. X. Geng, Q. Zhong, Structure–activity Relationship of Cr/Ti-PILC Catalysts using A Pre-modification Method for NO Oxidation and their Surface Species Study, *Phy. Chem. Chem. Phys.*, 2015, **17**, 15036-15045.

[S6] J. C. S. Wu, Y. T. Cheng, In Stu FTIR Study of Photocatalytic NO Reaction on Photocatalysts under UV Irradiation, *J. Catal.*, 2006, **237**, 393-404.

[S7] Q. Yang, G. Q. Tan, L. X. Yin, W. L. Liu, B. X. Zhang, S. J. Feng, Y. Bi, Y. Liu, T. Liu, Z. Q. Wang, H. J. Ren, A. Xia, Full-spectrum Broad-spectrum Degradation of Antibiotics by $BiVO_4$@BiOCl Crystal Plane S-type and Z-type Heterojunctions, *Chem. Eng. J.*, 2023, **467**, 143450.

[S8] F. Liu, Y. Q. Wang, D. Xu, F. Sun, S. C. Zhang, W. L. Wang, X. Y. Li, W. S. Yu, H. Yu, X. T. Dong, Full-spectrum-responsive 1D/2D $BiVO_4$:Er^{3+},Yb^{3+}/BiOCl Core-shell S-scheme Heterostructure with Boosted Charge Transport and Redox Capacity for the Efficient Removal of Organic Pollutants, *Ceram. Int.*, 2023, **49**, 13371-13385.

[S9] Q. H. Li, M. Wang, J. Y. He, Y. W. Wang, In Situ Synthesis of Core-shell like $BiVO_4$/BiOCl Heterojunction with Excellent Visible-light Photocatalytic Activity, *Opt. Mater.*, 2023, **144**, 114266.

[S10] M. de la, Garza-Galván, P. Zambrano-Robledo, J. Vazquez-Arenas, I. Romero-Ibarra, et al., In Situ Synthesis of Au-decorated BiOCl/$BiVO_4$ Hybrid Ternary System with Enhanced Visible-light Photocatalytic Behavior, *Appl. Surf. Sci.*, 2019, **487**, 743-754.

[S11] D. D. Lv, D. F. Zhang, X. P. Pu, D. Z. Kong, Z. H. Lu, X. Shao, H. Y. Ma, J. M. Dou, One-pot Combustion Synthesis of $BiVO_4$/BiOCl Composites with Enhanced Visible-light Photocatalytic Properties, *Sep. Purif. Technol*., 2017, **174**, 97-103.

[S12] L. J. Song, Y. Y. Pang, Y. J. Zheng, C. F. Chen, L. Ge, Preparation and Enhanced Photocatalytic Activity of Porous BiOCl/$BiVO_4$ Microspheres via A Coprecipitation-Hydrothermal Method, *J. Alloys Compd*., 2017, **710**, 375-382.

[S13] L. W. Shan, Y. T. Liu, J. Suriyaprakash, C. G. Ma, Z. Wu, L. M. Dong, L. Z. Liu, Highly Efficient Photocatalytic Activities, Band Alignment of $BiVO_4$/BiOCl {001} Prepared by In Situ Chemical Transformation, *J. Mol. Catal. A Chem.,* 2016, **411**, 179-187.

[S14] C. C. Feng, D. H. Wang, B. J. Jin, Z. B. Jiao, The Enhanced Photocatalytic Properties of BiOCl/$BiVO_4$ p–n Heterojunctions via Plasmon Resonance of Metal Bi, *RSC Adv*., 2015, **5**, 75947-75952.

[S15] J. Cao, C. C. Zhou, H. L. Lin, B. Y. Xu, S. F. Chen, Surface Modification of m-$BiVO_4$ with Wide Band-gap Semiconductor BiOCl to Largely Improve the Visible Light Induced Photocatalytic Activity, *Appl. Surf. Sci*., 2013, **284**, 263-269.

[S16] R. Akbarzadeh, A. Asadi, P. O. Oviroh, T.-C. Jen, One-Pot Synthesized Visible Light-Driven BiOCl/AgCl/$BiVO_4$ n-p Heterojunction for Photocatalytic Degradation of Pharmaceutical Pollutants, *Mater.* 2019, **12**, 2297.

[S17] X. F. Yang, Y. T. Xu, S. Naraginti, X. Y. Wei, Enhanced Sulfamethazine Detoxification by A Novel BiOCl (110)/NrGO/$BiVO_4$ Heterojunction, *Environ. Res*., 2023, **232**, 116351.

[S18] T. Kansaard, K. N. Ishihara, W. Pecharapa, Characterization and Visible Light-Driven Photocatalytic Activity of $BiVO_4$/BiOCl/Bi_2S_3 Nanocomposites Prepared by Sonochemical Process, *Phys. Status Solidi A*, 2023, **220**, 2200447.